12-2014

Composition-dependent stability of the medium-range order responsible for metallic glass formation

Feng Zhang
Iowa State University and Ames Laboratory, fzhang@ameslab.gov

Min Ji
Iowa State University and Ames Laboratory

Xiao-Wei Fang
Iowa State University, Ames Laboratory, and University of Science and Technology of China

Yang Sun
Iowa State University and Ames Laboratory, yangsun@ameslab.gov

Cai-Zhuang Wang
Iowa State University and Ames Laboratory, wangcz@ameslab.gov

See next page for additional authors

Composition-dependent stability of the medium-range order responsible for metallic glass formation

Abstract
The competition between the characteristic medium-range order corresponding to amorphous alloys and that in ordered crystalline phases is central to phase selection and morphology evolution under various processing conditions. We examine the stability of a model glass system, Cu–Zr, by comparing the energetics of various medium-range structural motifs over a wide range of compositions using first-principles calculations. We focus specifically on motifs that represent possible building blocks for competing glassy and crystalline phases, and we employ a genetic algorithm to efficiently identify the energetically favored decorations of each motif for specific compositions. Our results show that a Bergman-type motif with crystallization-resisting icosahedral symmetry is energetically most favorable in the composition range $0.63 < xCu < 0.68$, and is the underlying motif for one of the three optimal glass-forming ranges observed experimentally for this binary system (Li et al., 2008). This work establishes an energy-based methodology to evaluate specific medium-range structural motifs which compete with stable crystalline nuclei in deeply undercooled liquids.

Keywords
Metallic glass, Medium-range order, Genetic algorithm

Comments
This is a manuscript of an article published as Zhang, Feng, Min Ji, Xiao-Wei Fang, Yang Sun, Cai-Zhuang Wang, Mikhail I. Mendelev, M. J. Kramer, Ralph E. Napolitano, and Kai-Ming Ho. "Composition-dependent stability of the medium-range order responsible for metallic glass formation." *Acta Materialia* 81 (2014): 337-344. DOI: 10.1016/j.actamat.2014.08.041. Posted with permission.

Authors
Feng Zhang, Min Ji, Xiao-Wei Fang, Yang Sun, Cai-Zhuang Wang, Mikhail I. Mendelev, Matthew J. Kramer, Ralph E. Napolitano, and Kai-Ming Ho

111Equation Chapter 1 Section 1Composition-dependent stability of the medium-range order responsible for metallic glass formation

Feng Zhang,[1,2] Min Ji,[1,2] Xiao-Wei Fang,[1,2,3] Yang Sun,[1,2] Cai-Zhuang Wang,[1,2] Mikhail I. Mendelev,[1] M. J. Kramer,[1,4] Ralph E. Napolitano,[1,4] Kai-Ming Ho[1,2]

[1]Ames Laboratory, US Department of Energy, Ames, Iowa 50011, USA
[2]Department of Physics and Astronomy, Iowa State University, Ames, Iowa 50011, USA
[3]Hefei National Laboratory for Physical Sciences at Microscale and Department of Physics, University of Science and Technology of China, Hefei, Anhui 230026, People's Republic of China
[4]Department of Materials Science and Engineering, Iowa State University, Ames, Iowa 50011, USA

Abstract

The competition of characteristic medium range order corresponding to amorphous alloys and those in ordered crystalline phases is central to phase selection and morphology evolution under various processing conditions. We examine the stability of a model glass system, Cu-Zr, by comparing the energetics of various medium-range structural motifs over a wide range of compositions using first-principles calculations. We focus specifically on motifs that represent possible building blocks for competing glassy and crystalline phases, and we employ a genetic algorithm to efficiently identify the energetically favored decorations of each motif for specific compositions. Our results show that a Bergman-type motif with crystallization-resisting icosahedral symmetry is

energetically most favorable in the composition range $0.63 < x_{Cu} < 0.68$, and is the underlying motif for one of the three optimal glass-forming ranges observed experimentally for this binary system [1]. This work establishes an energy-based methodology to evaluate specific medium-range structural motifs which compete with stable crystalline nuclei in deeply undercooled liquids.

Key words: metallic glass; medium-range order; genetic algorithm.

1. Introduction

Metallic glasses are typically formed in bulk by rapid cooling from liquid melts. Within specific compositions [2], unstable or metastable structures may be effectively stabilized by extremely sluggish relaxation kinetics. A large number of such metallic glasses have been identified, and found applications because of their superior mechanical stiffness, strength, and chemical stability relative to their crystalline counterparts. Various phenomenological rules have been formulated to interpret the glass formability for metallic systems [3-6]. However, atomistic modeling of amorphous alloys is challenging due to the lack of periodic order. While thermodynamic stability of crystalline intermetallic phases can be readily and accurately described because of their well-defined crystalline order, for disordered systems, simulations on much larger time and length scales are required for proper statistical averaging.

The composition-dependent stability of metallic glass is poorly understood within existing theoretical framework. Some thermodynamic models predict the glass-forming composition range by comparing the energy of the disordered glassy state against the energy of a solid solution in the solvent lattice [7, 8]. However, a more relevant comparison can be made using complex intermetallic compounds as the reference state [9], especially when the solute and solvent have large size disparities or the solute concentration is high. Moreover, most of this work is empirical and not based on accurate energetic calculations, which is required to reliably establish phase stability. In addition, existing first-principles modeling of metallic glass is mainly based on ab-initio molecular dynamics (AIMD), whose capabilities are limited because of a large mismatch between experimental and computational time scales: Experimental melt-quenching time is usually of the order of milliseconds: orders of magnitude longer than what can be achieved in

AIMD. This mismatch results in significantly under-evolved structural configurations in computer simulations.

An emerging consensus is that metallic glass displays short to medium range order arising from the packing of local clusters [10-19]. This suggests that the stability of certain local motifs can be used to characterize the energetic stability of the glassy system. In this way, the energetic stability of a metallic glass can be estimated without *a priori* detailed knowledge of the amorphicity of the glass. Rather than focusing on a single detailed solution to the structure, which is not unique, our approach aims to capture the essential components of local order, which collectively govern the overall stability and physical properties of the bulk glass. Such a treatment also results in a significant reduction in the size of the calculated system, allowing the use of accurate first-principles methods.

2. Model and Simulation Details

2.1. Medium-range structural motifs in the Cu-Zr system

As an example, we examine the relative stability of various structural motifs in the Cu-Zr system which displays strong glass formability for a wide range of compositions [1, 20-23]. The Cu-Zr system has three optimal glass-forming regions with the Cu composition (x_{Cu}) around 0.50, 0.56 and 0.64 [1]. The composition-dependent glass formability has been attributed to the density of the amorphous phase [1], or a rationally designed parameter integrating the mixing enthalpy, the driving force for decomposition, and the excessive atomic space [24]. However, neither of these

approaches fully accounts for the chemical and topological medium-range order responsible for glass formation.

We consider both crystallization-favoring and crystallization-resisting motifs. Motifs collected from known Cu-Zr compounds are labeled as crystallization-favoring motifs. For the Cu-Zr system, simulations have demonstrated that local icosahedral clustering correlates with glass formation from the liquid state for certain compositions [10, 15, 17]. Because of the five-fold symmetry, the icosahedral cluster is not a space-filling motif, and is geometrically frustrating for crystalline packing. Therefore, icosahedral motifs are regarded as crystallization-resisting motifs. The effects of pentagonal short-range order with the five-fold symmetry on glass transition were examined in a two-dimensional toy model, using an interatomic potential artificially designed to favor the pentagonal packing [25]. Here, we focus on a real material, making no pre-assumption on the nature of the interactions in the system. In addition, we consider not only the first atomic shell (short-range order), but the next several atomic shells in order to include the full medium-range order [14]. For energy stability studies, these motifs need to be embedded in an atomic network, since the stability of stand-alone clusters is dominated by unsaturated atoms at the surface, which are irrelevant in well-packed solids. The atomic network is chosen to be periodic to facilitate computation. For crystalline-favoring motifs, all known stable and metastable structures in the phase diagram are tested. For icosahedral motifs, we choose quasicrystal approximant structures representing several typical medium-range icosahedral order [26, 27]. The physical and chemical properties of the approximant structures highly resemble those of the quasicrystals with the same local icosahedral clusters, suggesting that these local clusters play a dominant role in determining the properties of such aperiodic materials. Therefore, the approximant

structures should be good descriptors for metallic glasses with strong local icosahedral order as well.

The crystalline-favoring motifs considered are extracted from the compounds $CuZr_2$ (I4/mmm), CuZr (Pm3m), $Cu_{10}Zr_7$ (Aba2), Cu_8Zr_3 (Pnma), $Cu_{51}Zr_{14}$ (P6/m), and Cu_5Zr ($F\bar{4}3m$) [28]. The space group nomenclature is given in the brackets, which establishes the packing feature of each motif based on the details of the atomic decoration for each compound. In addition, four icosahedral motifs are included, which are derived from quasicrystal approximants $Mg_{32}(Al, Zn)_{49}$ [29], α(AlMnSi) [30], $YbCd_6$ [31] and $MoAl_{12}$ [32], as shown in Fig. 1 (a), (b), (c) and (d), respectively. $Mg_{32}(Al, Zn)_{49}$, $YbCd_6$ and $MoAl_{12}$ all have bcc lattices, and α(AlMnSi) also has a nearly bcc structure. Thus, the structures in Fig. 1 are bounded by the Wigner-Seitz unit cell of the bcc lattice, which has the shape of a truncated octahedron. Figure 1 (a), (b), (c) represent the Bergman-type [29], Mackay-type [33], and Tsai-type [34] icosahedral motifs, respectively. The icosahedral motif shown in Fig. 1 (d) will be referred to as MoAl-type, whose characteristic feature is a network of non-interpenetrating icosahedra.

2.2. Iterative genetic-algorithm (GA) search

We study the relative stability of these crystalline-favoring motifs and icosahedral motifs for a wide range of Cu compositions ($0.25 < x_{Cu} < 0.85$). For each motif, the Bravais lattice and the atomic sites are predetermined by a template structure as discussed above. What remains to be decided is the energetically most favorable decoration of the

template with Cu and Zr atoms according to a specific x_{Cu}. We use a global GA search [35, 36] to perform this task, which is carried out separately for each motif at each composition. The initial pool for the GA search contains a number of structures that share the same template and composition but have randomly generated arrangements of Cu and Zr atoms. The energy of each structure is evaluated as its fitness. The structures are allowed to relax during the energy calculations. While these relaxations create some geometric distortions, the key topological features of the motif will be maintained. Then, "parents" are selected primarily from structures with relatively low energies to create next-generation structures based on a "cut-and-paste" mating operation, as schematically illustrated in Fig. 2 [35, 36]. We use the unrelaxed structures representing different decorations during the mating process. The structures with the highest energies in the pool will be replaced by the next-generation structures that have better fitness values. The above process is repeated until the structure pool stops evolving.

For each motif, the GA search is carried out in unit cells with about 100 atoms, allowing us to vary the composition of the system with a fine interval of approximately one percent. Such large unit cells are time-consuming if first-principles calculations are used throughout the search. Thus it is necessary to adopt a more efficient auxiliary potential for energy calculations during the GA search. Here, we choose an interatomic potential in the Finnis-Sinclair (FS) form [37], that has been commonly used to model the Cu-Zr system [38]. The FS potential can be expressed as

22* MERGEFORMAT ()

$$U = \sum_{i<j} \phi^{\alpha_i \alpha_j}(r_{ij}) + \sum_i \Phi^{\alpha_i}(\rho_i).$$

In Eq. 1, α^i denotes the type of atom *i*, and r_{ij} is the separation between atoms *i* and *j*. $\phi^{\alpha_i\alpha_j}(r_{ij})$ is the energy for the pairwise interaction between atoms *i* and *j*, and $\Phi^{\alpha_i}(\rho_i)$ is the energy for embedding an atom with type α_i at a position with a background charge density ρ_i, which can be further expressed as

$$\rho_i = \sum_j \psi^{\alpha_i\alpha_j}(r_{ij}), \qquad 33\backslash* \text{ MERGEFORMAT ()}$$

where $\psi^{\alpha_i\alpha_j}$ represents the contribution of atom *j* to the background charge density at the position of atom *i*.

While the FS potential is sufficiently fast, it was developed to fit a broad range of thermodynamic parameters [38]. We check the FS potential with more accurate density functional theory (DFT), as implemented in the VASP package [39, 40]. The generalized gradient approximation proposed by Perdew, Burke, and Ernzerhof [41] is used for the exchange-correlation functional. The electron-ion interaction is treated with the projector-augmented wave method [42]. A cut-off energy of 400 eV is used for the plane-wave basis. The total-energy converges to 10^{-5} eV per cell in each self-consistent

loop, and the structural relaxation terminates when the force on each atom is smaller than 0.01 eV/Å.

Fig. 3 (a) compares the formation energies (E_{form}) calculated by FS and DFT for structures collected at $x_{\text{Cu}} = 0.65$ for all structural motifs. E_{form} is defined as the total energy of a structure referenced to the phase separated mixture of pure Cu and pure Zr. As one can see, there exist significant disagreements between the relative stability of the motifs calculated by DFT and that calculated by the original FS potential.

To correct these discrepancies, we adjust the FS potential at a fixed composition, using the following approach: DFT checks are performed after each GA search, and the DFT results are used to refine the FS potential by minimizing a weighted combination of the mismatches in energies, forces and stresses calculated by DFT and FS, using the POTFIT program [43, 44], Then a new GA search is performed with the refined FS potential. If structures with lower energies are found in the new GA search, these structures are added to the potential-refinement process. The above cycle is repeated until the GA search converges. About 30 structures for each motif (a total pool of over 300 structures) are used in the refinement process. This process is performed separately for a series of different Cu compositions to obtain accurate FS potentials over the whole stoichiometric range. The formation energies of the low-energy structures at $x_{\text{Cu}} = 0.65$ calculated by DFT and the refined FS potential are shown in Fig. 3 (b). Compared with Fig. 3 (a), the agreement between DFT and FS is greatly improved.

3. Results and Discussions

3.1 Energetic stability of medium-range motifs as a function of the composition

Besides $x_{\mathrm{Cu}} = 0.65$, the iterative GA search is performed for several other Cu compositions x_{Cu} = 0.33, 0.5, 0.69, 0.73, 0.78, and 0.83, where stable Cu-Zr compounds exist. Low-energy structures as well as refined FS potentials are thus obtained at these compositions as well. We have provided the refined FS potentials in Supplementary Material. For each motif, we perform GA searches for Cu compositions ranging from 0.25 to 0.85 with interval of about 0.01 (the exact interval depends on the size of the supercell). At each composition, we use a FS potential interpolated from the refined potentials at nearby compositions. Figure 4 (a) shows the results of these extensive GA searches. DFT calculations are performed on the low-energy structures found in each GA search, and the formation energy is calculated based on the lowest DFT energy. Only the most stable crystalline-favoring motif at each Cu composition is shown in Fig. 4 (a) for easier viewing. At each Cu composition where there exists a line compound in the Cu-Zr phase diagram in Fig. 4 (b), the crystallization-favoring motif characterized by the compound is found to be the most favorable structural order.

In the composition range $0.63 < x_{Cu} < 0.68$, the Bergman-type icosahedral motif is the most stable medium-range order, and is responsible for glass formation due to its crystallization-resisting nature. This composition range compares favorably with one of the three optimal glass formation ranges observed in experiments [1]. On the other hand,

no icosahedral motifs are stable outside of this composition range. Therefore, our results exclude icosahedral ordering as the fundamental reason for the glass formation at other composition ranges. Several other works that used the Voronoi tessellation technique to analyze the structures of Cu-Zr glasses generated by molecular dynamics (MD) simulations also showed strong composition dependence of the icosahedral order [45-47]. The Cu composition for optimal icosahedral order established in such work varies from 0.65 to 0.75, possibly due to the different interatomic potentials used in the MD simulations. The other icosahedral motifs are significantly less stable than the Bergman-type icosahedral motif, although they share similar short-range icosahedral clusters (except for the Tsai-type motif which has a tetrahedron core), indicating that medium-range order up to the second shell and beyond is important in the atomic arrangements of metallic glasses. At $0.63 < x_{Cu} < 0.68$, the approximant structures used to model the Bergman-type icosahedral motif are unstable against phase separation into the equilibrium mixture of $Cu_{10}Zr_7$ and Cu_8Zr_3, since the formation energy of the Bergman approximant structures in this composition range [thick red line in Fig. 4 (a)] is above the tie line connecting the equilibrium $Cu_{10}Zr_7$ and Cu_8Zr_3 phases [dash-dotted line in Fig. 4 (a)]. This phase separation requires long-range transport of Cu and Zr atoms, which cannot be achieved under ultra-fast quenching conditions. Moreover, it also takes significant time for local Bergman clusters to arrange into a periodic network; thus, with fast quenching, even the approximant structures themselves can hardly be reached. However, since local atomic packing is a fast process, a significant fraction of local Bergman-type clusters can be formed given that they are energetically favorable.

3.2. Effects of the configurational entropy

The GA search that we have performed also allows us to estimate the configurational entropy originated from different decorations of the lattice structures. A large number of inequivalent decorations are generated during the course of a complete genetic-algorithm search. These structures form a reasonable pool for sampling the entire configurational space. Therefore, the free energy, including the contributions from the configurational entropy, can be estimated from the equation

$$e^{-F/k_BT} = \sum_i e^{-E_i/k_BT}, \qquad 44\backslash* \text{ MERGEFORMAT ()}$$

where F is the free energy; k_B is the Boltzmann constant; T is the temperature; E_i is the energy of each decoration; and i sums over all inequivalent decorations visited during the GA search.

Taking the Bergman-type approximant structure as an example, over 10,000 structures with different atomic decorations are generated during the GA search for the ground state with the Bergman-type motif at $x_{\mathrm{Cu}} \sim 0.65$. Figure 5 (a) gives the density of states sampled from these structures, where it can be seen that the energies for these structures span multiple electronvolts per unit cell (containing 81 atoms). The large difference in energies for structures with different decorations is caused by the differential atomic size and chemical properties between the Cu and Zr elements. Most of these structures make negligible contributions to the free energy, since their energy separation

from the ground state is much larger than $k_B T$ (~0.03 eV at room temperature). As a result, the total contribution from the configurational entropy, calculated by $F - E_0$ (E_0 is the ground state energy), is only about 1 meV/atom at room temperature, as shown in Fig. 5 (b). As shown in Fig. 4 (a), the structure representing the Bergman-type motif is at least 0.02 eV/atom more stable than other structures at $x_{\mathrm{Cu}} \sim 0.65$. Therefore, the small contributions from the configurational entropy do not qualitatively affect the stability of the Bergman-type motif.

3.3. Preference of Bergman MRO in rapidly cooled samples

To verify that the Bergman-type order remains preferred under kinetic effects, we have performed Molecular Dynamics (MD) simulations on rapidly cooled $Cu_{65}Zr_{35}$ system. The unit cell contains 5,000 atoms with periodic boundary conditions. The refined FS potential at this composition is used for energy calculations. The samples are first melted and equilibrated at T = 1500 K, and then cooled to T = 300 K at four different cooling rates: 5×10^{12}, 5×10^{11}, 5×10^{10}, and 5×10^{9} K/s. To study the local order in a glassy sample, a cluster around each atom is extracted from the sample and aligned against an ideal template, using the method described in Ref. [13]. For the Bergman, Mackay and Tsai-type icosahedral motifs, the templates are given in the left panels of

Fig. 1 (a)–(c), respectively, which all contain multiple atomic shells. For the MoAl-type, since the unit cell is made of a single icosahedron [see the left panel of Fig. 1 (d)], we choose two templates to represent two possible connections of neighboring icosahedra with a square or an octahedron, as shown in the right panel of Fig. 1 (d). In addition, the crystalline-favoring templates for the two crystalline phases with neighboring compositions $Cu_{10}Zr_7$ (Aba2) and Cu_8Zr_3 (Pnma) are also tested, in order to check whether the quenched sample contains nucleates of these two crystals. An alignment score, describing how an as-extracted cluster deviates from a perfect template, is defined as

55* MERGEFORMAT ()

$$f = \left(\frac{\sum_{i=1}^{N} \left| r_{ic} - r_{it} \right|^2}{N r_0^2} \right)^{1/2}$$

where N is the number of the atoms in the template, r_0 is the typical bond length of the template, r_{ic} and r_{it} are the atom positions in the aligned cluster and template, respectively. The smaller the alignment score is, the less deviation the cluster has compared with the template. Figure 6 (a) shows the cumulative distributions of the alignment score obtained by aligning all the clusters in the sample prepared at the slowest cooling rate 5×10^9 K/s against different templates. It is clear that the sample displays much better Bergman-type

order than other types of icosahedral orders. The sample contains a very low population of Aba2 and Pnma type crystalline-favoring clusters, indicating that the glassy sample is free of nucleates of these crystalline phases. Figure 6 (b) plots the cumulative distribution of the alignment score against the Bergman template for samples cooled at different cooling rates. The fraction of Bergman-like clusters increases as the cooling rate decreases. Since our cooling rates are still much faster than those used in experiments, we expect actual fraction of Bergman clusters in real Cu-Zr glasses to be even higher than our simulations. With the gradual enhancement of Bergman-type order as the cooling process is slowing down, the internal energy of the glass is also decreasing, as shown in the inset of Fig. 6 (b). This reconfirms that the Bergman-type motif is energetically favorable in the Cu-Zr glass at $x_{\mathrm{Cu}} \sim 0.65$.

Several previous studies of CuZr-based glasses establish that the local icosahedral clusters up to the first shell are connected into an interpenetrating network [18, 48-50], in which two adjacent icosahedral clusters share a pentagonal bipyramid. The Bergman-type MRO also features similar interpenetrating connection. In an ideal Bergman motif [Fig. 1 (a)], a central icosahedral cluster is inter-connected to 12 outer icosahedral clusters, forming a "star-like" icosahedral suopercluster. Our molecular dynamics simulations show that a decreasing cooling rate promotes this connected Bergman order and enhances the icosahedral "star-like" network. Further clustering of Bergman motifs, which could provide useful information about the longer-range correlations of the system, can also be studied in MD simulations [14]. Unfortunately, to evaluate the energetic stablity of such clustering in the current GA-based method requires a unit cell containing multiple

Bergman motifs, which exceeds the capability of global optimization-based structure prediction methods, even with the help of efficient interatomic potentials. (The difficulty of such problems grows exponentially with the system size).

4. Conclusions

In conclusion, we have developed a new method to characterize the stability of local medium-range order in metallic glasses with accurate first-principles calculations. This method enables us to clarify from a pure energetic point of view the origin for the selection of local structural order, which ultimately determines glass formation in deeply undercooled metallic liquids. The Cu-Zr is an ideal model system to demonstrate the relative stability of various medium-range structural orders as a function of the composition. In the optimal glass-forming region with x_{Cu} around 0.65, a crystallization-resisting Bergman-type motif is not only more stable than the motifs existing in stable Cu-Zr compounds that are inclined to crystallization, but more stable than several other motifs with the same first-shell icosahedral order. Meanwhile, our results exclude icosahedral ordering as the fundamental reason for the glass formation in other composition ranges. A complete description of the Cu-Zr glass is still pending on the identification of the non-icosahedral structural motifs for the other glass-forming composition ranges. However, the method outlined in the paper is complete and generally applicable to any system where appropriate candidate motifs are available.

Acknowledgements

Work at Ames Laboratory was supported by the US Department of Energy, Basic Energy Sciences, Division of Materials Science and Engineering, under Contract No.

DE-AC02-07CH11358, including a grant of computer time at the National Energy Research Supercomputing Center (NERSC) in Berkeley, CA. F.Z. thank S.H. Zhou for preparing the Cu-Zr phase diagram.

References

[1] Li Y, Guo Q, Kalb JA, Thompson CV. Matching Glass-Forming Ability with the Density of the Amorphous Phase. Science 2008;322:1816.

[2] Greer AL. Confusion by design. Nature 1993;366:303.

[3] Turnbull D. A. Structure Informationamorphous Solid Formation and Interstitial Solution Behavior in Metallic Alloy Systems. Le Journal de Physique Colloques 1974;35:C4.

[4] Egami T, Waseda Y. Atomic Size Effect on the Formability of Metallic Glasses. J. Non·Cryst. Solids 1984;64:113.

[5] Takeuchi A, Inoue A. Classification of Bulk Metallic Glasses by Atomic Size Difference, Heat of Mixing and Period of Constituent Elements and Its Application to Characterization of the Main Alloying Element. JIM, Materials Transactions 2005;46:2817.

[6] Lu ZP, Liu CT, Wu Y, Tan H, Li Y, Chen GL. Composition Effects on Glass-Forming Ability and its Indicator γ. Intermetallics 2008;16:410.

[7] Weeber AW, Bakker H. Amorphization by Ball Milling. A review. Physica B: Condensed Matter 1988;153:93.

[8] Gallego LJ, Somoza JA, Alonso JA, Lopez JM. Prediction of the Glass Formation Range of Transition Metal Alloys. J. Phys. F: Met. Phys. 1988;18:2149.

[9] Xia L, Fang SS, Wang Q, Dong YD, Liu CT. Thermodynamic Modeling of Glass Formation in Metallic Glasses. Appl. Phys. Lett. 2006;88.

[10] Sheng H, Luo W, Alamgir F, Bai J, Ma E. Atomic Packing and Short-to-Medium-Range Order in Metallic Glasses. Nature 2006;439:419.

[11] Luo W, Sheng H, Alamgir F, Bai J, He J, Ma E. Icosahedral Short-Range Order in Amorphous Alloys. Phys. Rev. Lett. 2004;92.

[12] Cheng YQ, Ma E. Indicators of Internal Structural States for Metallic Glasses: Local Order, Free Volume, and Configurational Potential Energy. Appl. Phys. Lett. 2008;93:51910.

[13] Fang X, Wang C, Yao Y, Ding Z, Ho K. Atomistic Cluster Alignment Method for Local Order Mining in Liquids and Glasses. Phys. Rev. B 2010;82:184204.

[14] Fang XW, Wang CZ, Hao SG, Kramer MJ, Yao YX, Mendelev MI, Ding ZJ, Napolitano RE, Ho KM. Spatially Resolved Distribution Function and the Medium-Range Order in Metallic Liquid and Glass. Sci. Rep. 2011;1:194.

[15] Hwang J, Melgarejo ZH, Kalay YE, Kalay I, Kramer MJ, Stone DS, Voyles PM. Nanoscale Structure and Structural Relaxation in Zr_{50}Cu_{45}Al_{5} Bulk Metallic Glass. Phys. Rev. Lett. 2012;108.

[16] Miracle DB. A Structural Model for Metallic Glasses. Nature Mater. 2004;3:697.

[17] Wang XD, Lou HB, Gong Y, Vainio U, Jiang JZ. Heterogeneities in CuZr-Based Bulk Metallic Glasses Studied by X-ray Scattering. J. Phys.: Condens. Matt. 2011;23:075402.

[18] Li M, Wang C, Hao S, Kramer M, Ho K. Structural Heterogeneity and Medium-Range Order in $Zr_x Cu_{100-x}$ Metallic Glasses. Phys. Rev. B 2009;80:184201.

[19] Hirata A, Guan P, Fujita T, Hirotsu Y, Inoue A, Yavari AR, Sakurai T, Chen M. Direct Observation of Local Atomic Order in a Metallic Glass. Nat. Mater. 2011;10:28.

[20] Xu D, Lohwongwatana B, Duan G, Johnson WL, Garland C. Bulk Metallic Glass Formation in Binary Cu-rich Alloy Series – $Cu_{100-x}Zr_x$ (x=34, 36, 38.2, 40 at.%) and Mechanical Properties of Bulk $Cu_{64}Zr_{36}$ Glass. Acta Mater. 2004;52:2621.

[21] Tang M-B, Zhao D-Q, Pan M-X, Wang W-H. Binary Cu-Zr Bulk Metallic Glasses. Chin. Phys. Lett. 2004;21:901.

[22] Wang D, Li Y, Sun BB, Sui ML, Lu K, Ma E. Bulk Metallic Glass Formation in the Binary Cu–Zr System. Appl. Phys. Lett. 2004;84:4029.

[23] Inoue A, Zhang W. Formation, Thermal Stability and Mechanical Properties of Cu-Zr and Cu-Hf Binary Glassy Alloys Rods. Mech. Trans. 2004;45:584.

[24] Yu CY, Liu XJ, Lu J, Zheng GP, Liu CT. First-Principles Prediction and Experimental Verification of Glass-Forming Ability in Zr-Cu Binary Metallic Glasses. Sci. Rep. 2013;3:2124.

[25] Shintani H, Tanaka H. Frustration on the Way to Crystallization in Glass. Nat. Phys. 2006;2:200.

[26] Goldman A, Kelton R. Quasicrystals and Crystalline Approximants. Rev. Mod. Phys. 1993;65:213.

[27] Tsai AP. Icosahedral Clusters, Icosaheral Order and Stability of Quasicrystals—a View of Metallurgy. Science and Technology of Advanced Materials 2008;9:013008.

[28] Okamoto H. Cu-Zr (Copper-Zirconium). Journal of phase equilibria and diffusion 2008;29:204.

[29] Bergman G, Waugh JLT, Pauling L. The Crystal Structure of the Metallic Phase Mg32(Al, Zn)49. Acta Cryst. 1957;10:254.

[30] Cooper M, Robinson K. The Crystal Structure of the Ternary Alloy α(AlMnSi). Acta Cryst. 1966;20:614.

[31] Palenzona A. The Ytterbium Cadmium System. Journal of the Less-Common metals 1971;25:367.

[32] Adam J, Rich JB. The Crystal Structure of WAl12, MoAl12 and (Mn, Cr)Al12. Acta Crystallogr. 1954;7:813.

[33] Mackay A. A Dense Non-Crystallographic Packing of Equal Spheres. Acta Cryst. 1962;15:916.

[34] Tsai AP, Guo JQ, Abe E, Takakura H, Sato TJ. Alloys: A Stable Binary Quasicrystal. Nature 2000;408:537.

[35] Deaven D, Ho K. Molecular Geometry Optimization with a Genetic Algorithm. Phys. Rev. Lett. 1995;75:288.

[36] Ji M, Wang CZ, Ho KM. Comparing Efficiencies of Genetic and Mimimal Hopping Algorithms for Crystal Structure Prediction. Physical Chemistry Chemical Physics 2010;12:11617.

[37] Finnis M, Sinclair J. A Simple Empirical N-body Potential for Transition Metals. Phil. Mag. A 1984;50:45.

[38] Mendelev MI, Kramer MJ, Ott RT, Sordelet DJ, Yagodin D, Popel P. Development of Suitable Interatomic Potentials for Simulation of Liquid and Amorphous Cu–Zr Alloys. Philos. Mag. 2009;89:967.

[39] Kresse G, Furthmüller J. Efficient Iterative Schemes for *ab initio* Total-Energy Calculations Using a Plane-Wave Basis Set. Phys. Rev. B 1996;54:11169.

[40] Kresse G, Furthmüller J. Efficiency of ab-initio Total Energy Calculations for Metals and Semiconductors Using a Plane-Wave Basis Set. Computational Materials Science 1996;6:15.

[41] Perdew JP, Burke K, Ernzerhof M. Generalized Gradient Approximation Made Simple. Phys. Rev. Lett. 1996;77:3865.

[42] Vanderbilt D. Soft Self-Consistent Pseudopotentials in a Generalized Eigenvalue Formalism. Phys. Rev. B 1990;41:7892.

[43] Peter B, Franz G. Potfit: Effective Potentials from ab initio Data. Modelling and Simulation in Materials Science and Engineering 2007;15:295.

[44] Brommer P, Gähler F. Effective Potentials for Quasicrystals from ab-initio Data. Philos. Mag. 2006;86:753.

[45] Mendelev M, Kramer M, Ott R, Sordelet D, Besser M, Kreyssig A, Goldman A, Wessels V, Sahu K, Kelton K. Experimental and Computer simulation Determination of the Structural Changes Occurring through the Liquid–Glass Transition in Cu–Zr Alloys. Phil. Mag. 2010;90:3795.

[46] Ward L, Miracle D, Windl W, Senkov ON, Flores K. Structural Evolution and Kinetics in Cu-Zr Metallic Liquids from Molecular Dynamics Simulations. Phys. Rev. B 2013;88:134205.

[47] Wakeda M, Shibutani Y, Ogata S, Park J. Relationship between Local Geometrical Factors and Mechanical Properties for Cu–Zr Amorphous Alloys. Intermetallics 2007;15:139.

[48] Tomida T, Egami T. Molecular-Dynamics Study of Orientational Order in Liquids and Glasses and its Relation to the Glass Transition. Phys. Rev. B 1995;52:3290.

[49] Hui X, Fang HZ, Chen GL, Shang SL, Wang Y, Liu ZK. Icosahedral Ordering in $Zr_{41}Ti_{14}Cu_{12.5}Ni_{10}Be_{22.5}$ Bulk Metallic Glass. Appl. Phys. Lett. 2008;92:201913.

[50] Wakeda M, Shibutani Y. Icosahedral Clustering with Medium-Range Order and local Elastic Properties of Amorphous Metals. Acta Materialia 2010;58:3963.

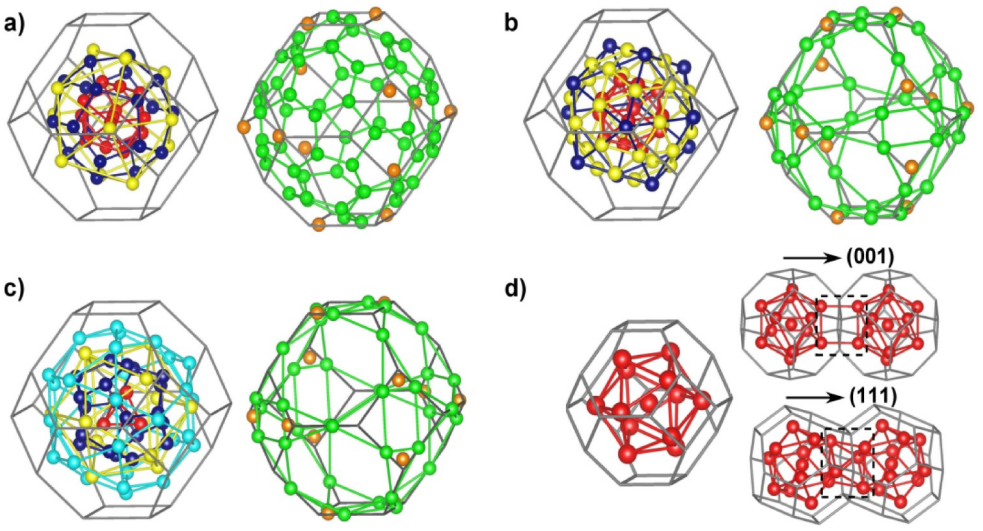

Fig. 1. Medium-range icosahedral order in typical quasicrystal approximants with bcc lattice. (a) $Mg_{32}(Al, Zn)_{49}$. Left: Bergman-type cluster inside the Wigner-Seitz unit cell, comprised of an icosahedron with the center occupied (red), a dodecahedron (blue), and a larger icosahedron (yellow). Right: Atoms on the surface of the unit cell including a 60-atom buckyball (green) and 12 additional atoms (pink) above 12 hexagons of the buckyball. (b) α(AlMnSi). Left: Mackay-type cluster inside the unit cell comprised of an icosahedron with the center vacant (red), a larger icosahedron twice the size of the first one (blue), and an icosidodecahedron (yellow). Right: atoms on the surface of the cell including 24 atoms on the edges of the truncated-octahedral unit cell (green), and 12 orange atoms close to the face diagonals of the squares. In α(AlMnSi), the orange atoms form a simple cubic lattice, that is, the body-centered counterparts are missing. However, when this structure is translated to the Cu-Zr system, adding the missing atoms results in more stable structures. (c) $YbCd_6$. Left: Tsai-type cluster inside the unit cell containing a central tetrahedron (red), a dodecahedron (blue), an icosahedron (yellow), and an icosidodecahedron (cyan). Right: atoms on the surface of the unit cell, similar to that in (b). (d) $MoAl_{12}$. Left: MoAl-type cluster which is an icosahedron with the center

occupied. Right: the connection of two neighboring icosahedra through a square (MoAl-Sq.) and an octahedron (MoAl-Octa.) along the (001) and (111) directions, respectively.

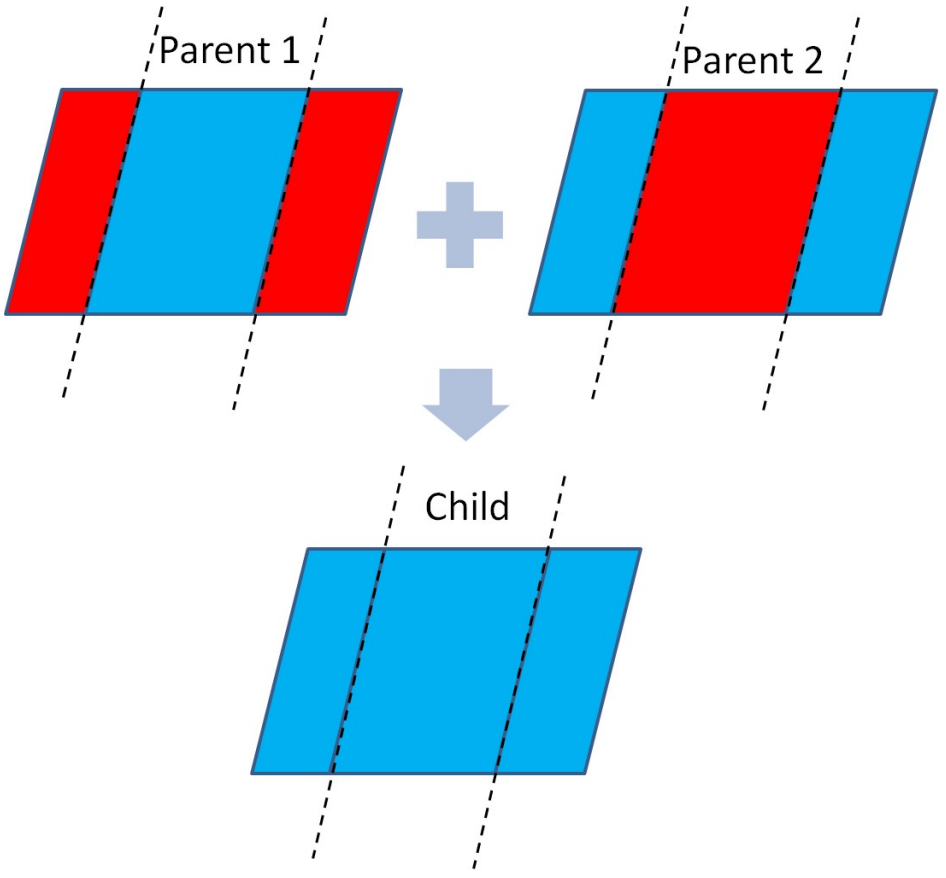

Fig. 2. Schematic illustration of the “cut-and-paste” mating operation in the GA search. In the current study, both parent structures have the same Bravais lattice and atomic sites, but have different atomic decorations. To perform the mating operation, we first create two bounding planes (dashed lines) to cut the parent structures into separate regions denoted by different colors. Then, a child structure is assembled by combining the atoms in the regions of the two parent structures that have the same color. Since this “cut-and-paste” operation can result in a different atomic composition from the desired value, if necessary, we finally apply a series of flipping operations (i.e., randomly changing a Cu atom to Zr and vice versa) to correct the composition.

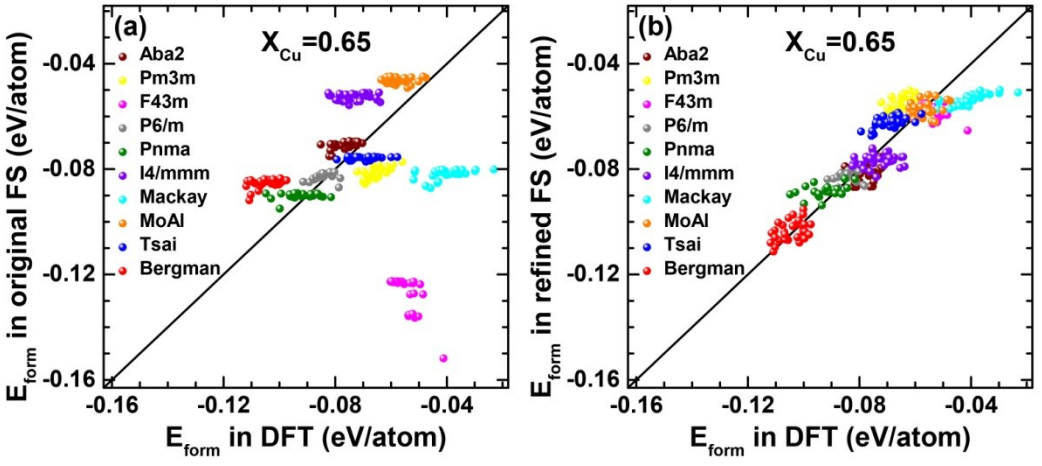

Fig. 3. Comparison of the formation energies calculated by (a) the original FS potential and (b) the refined FS potential with those calculated by DFT for the low-energy structures found in GA searches at $x_{Cu} \sim 0.65$.

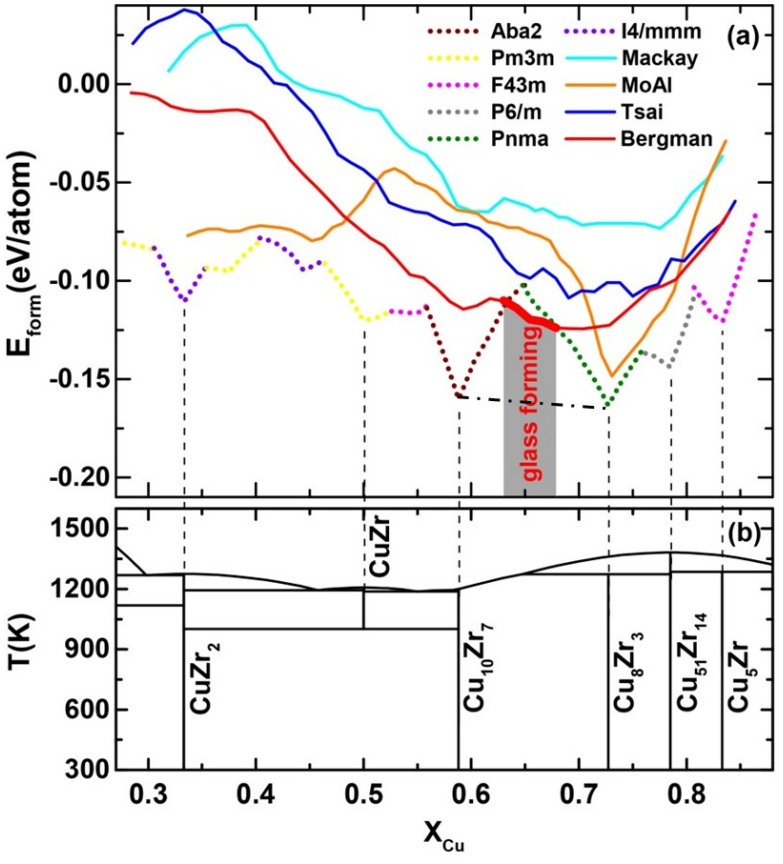

Fig. 4. (a) Formation energy of the lowest energy structure for each motif found in GA search, as a function of x_{Cu}. At each composition, only the most stable crystallization-favoring motif is shown for easier viewing. The bold red line highlights the composition range where the crystallization-resisting Bergman-type icosahedral motif is more energetically favorable than all crystallization-favoring motifs. The dash-dotted line is the tie line connecting the thermodynamically equilibrium $Cu_{10}Zr_7$ and Cu_8Zr_3 phases. (b) The phase diagram of the Cu-Zr system.

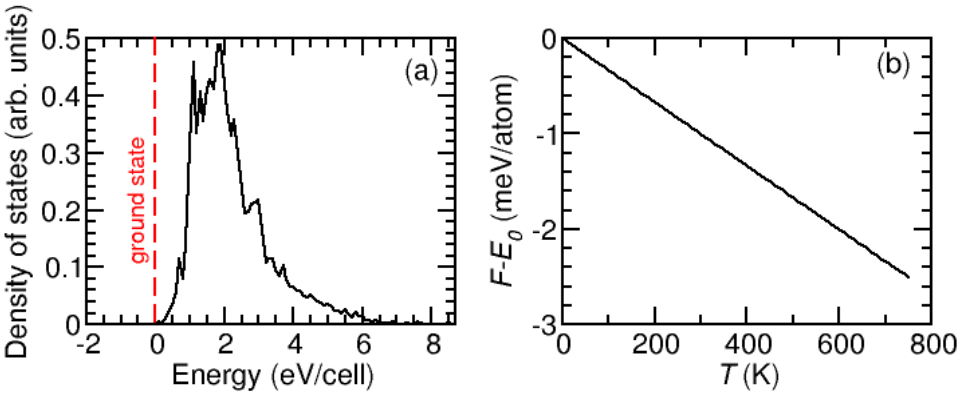
Density of states (arb. units)
0.5
0.4
0.3
0.2
0.1
0
-2
0
2
4
6
8
Energy (eV/cell)
ground state
(a)
F-E_0 (meV/atom)
0
-1
-2
-3
0
200
400
600
800
T (K)
(b)

Fig. 5. (a) Density of states for all the structure visited during the genetic-algorithm search for the optimal Bergman-type approximant structure at $x_{\mathrm{Cu}} \sim 0.65$. The unit cell contains 81 atoms. The energy of the ground state is set to be zero. (b) $F - E_0$ as a function of the temperature, where F and E_0 refer to the free energy and the ground-state energy, respectively.

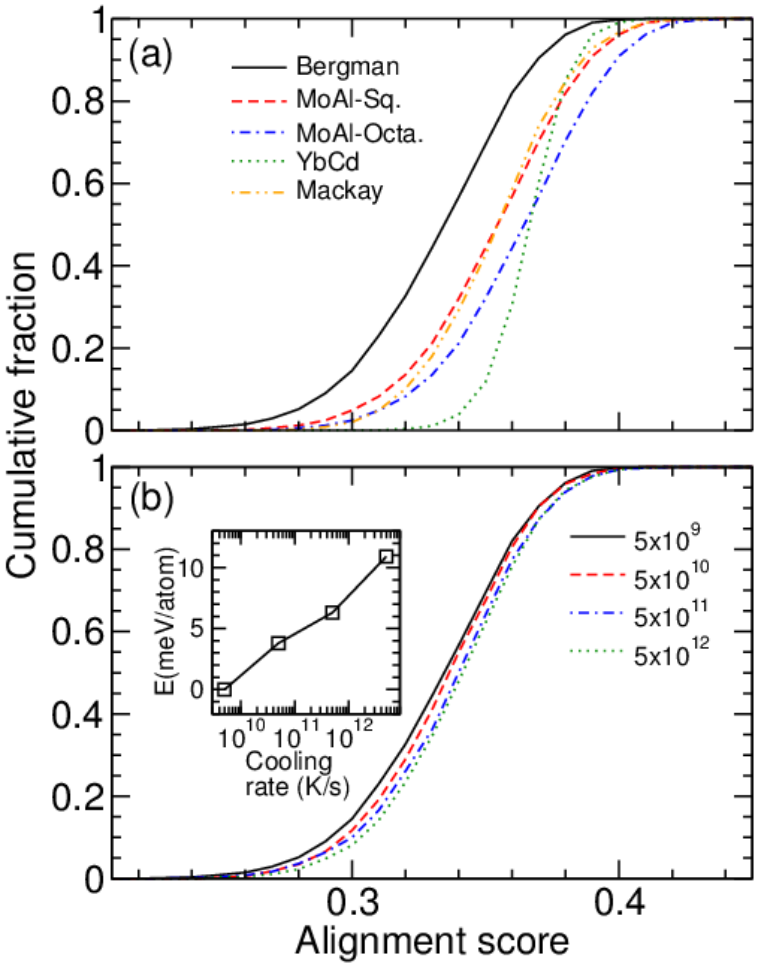

Fig. 6. (a) The cumulative distribution of the alignment score against different types of icosahedral templates for the sample prepared at a cooling rate of 5×10^{9} K/s. (b) The cumulative distribution of the alignment score against the Bergman template for samples prepared at different cooling rates. Inset: the internal energy of the sample at 300 K as a function of the cooling rate.